Experimental study on acoustic subwavelength imaging based on zero-mass metamaterials

2015 EPL 109 28001

(http://iopscience.iop.org/0295-5075/109/2/28001)

A Letters Journal Exploring the Frontiers of Physics

January 2015

EPL, **109** (2015) 28001
doi: 10.1209/0295-5075/109/28001

www.epljournal.org

Experimental study on acoustic subwavelength imaging based on zero-mass metamaterials

Xianchen Xu, Pei Li, Xiaoming Zhou[a] and Gengkai Hu

Key Laboratory of Dynamics and Control of Flight Vehicle, Ministry of Education and School of Aerospace Engineering, Beijing Institute of Technology - Beijing 100081, China

received 25 September 2014; accepted in final form 24 December 2014
published online 22 January 2015

PACS 81.05.Xj – Metamaterials for chiral, bianisotropic and other complex media
PACS 43.58.Ls – Acoustical lenses and microscopes
PACS 43.60.Lq – Acoustic imaging, displays, pattern recognition, feature extraction

Abstract – Anisotropic zero-mass acoustic metamaterials are able to transmit evanescent waves without decaying to a far distance, and have been used for near-field acoustic subwavelength imaging. In this work, we design and fabricate such metamaterial lens based on clamped paper membrane units. The zero-mass frequency is determined by normal-incidence acoustic transmission measurement. At this frequency, we verify in experiment that the fabricated metamaterial lens is able to distinguish clearly two sound sources separated with a distance $0.16\lambda_0$ (λ_0 is the wavelength in air) below the diffraction limit. We also demonstrate that the imaging frequency is invariant to the change of the lens thickness.

Introduction. – Acoustic waves which propagate in zero-mass media experience the zero-phase shift and quasi-static field distribution [1–3]. An interesting phenomenon arising from these properties is the extraordinary wave transmission. Complete transmission through zero-mass acoustic media is based on the impedance matching [4], which can compensate the mismatch introduced by the difference of geometric cross-sections, and thus allowing for a variety of exciting applications, including super tunneling in narrow channels [5], incident-angle–independent giant acoustic transmission [6], and constant transmission of acoustic evanescent waves used for subwavelength imaging [4].

The zero-mass transmission has first been demonstrated for lattice acoustic waves in a discrete linear chain constructed with spring connected resonators [1]. The vibration response measured at the end of the chain is in the same magnitude as the excitation at the resonator's zero-mass frequency. This is because of the vanishing inertial force from resonators with zero mass, and so does the undeformation of elastic springs between resonators. Acoustic zero-mass transmission was later observed in an air channel filled periodically with clamped elastic layers [4]. Clamped slabs produce effective mass density with the Drude-type expression [7]

$$\rho_{\text{eff}} = \rho(1 - \omega_{\text{c}}^2/\omega^2),$$

where zero mass is obtained at ω_{c}^2, which approaches the fundamental frequency of the clamped plate [8]. At zero-mass frequency, clamped layers in the channel oscillate with the same phase, and then the air cavities between adjacent layers are not deformed [9], leading to complete acoustic transmission; the effect is very similar to that observed in the lattice system. Fleury and Alù [5] find that acoustic waves emanating in a large tube can tunnel through a narrow channel filled with clamped membranes, and this zero-mass tunneling is independent of the channel length or the presence of bends and twists along the channel because of the quasi-static distribution of wave fields. Park *et al.* [6] demonstrate experimentally that zero-mass acoustic transmission observed in a rigid slab perforated with holes covering stretched soft membranes is independent on the sound incident angle.

In a previous work [4], the zero-mass effect has been used for complete transmission of acoustic evanescent waves, which always decay in normal materials. An anisotropic zero-mass metamaterial has been proposed to convert evanescent waves to propagating ones with the infinite-mass effect, and transfer them to the exit side of the lens structure based on the zero-mass transmission,

[a]E-mail: zhxming@bit.edu.cn

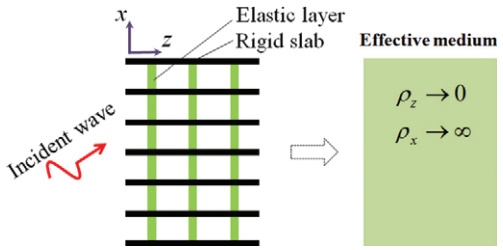

Fig. 1: (Colour on-line) The theoretical model of the lens made of rigid solid slabs with a periodic array of cavities partially filled by elastic layers.

realizing, finally, acoustic near-field subwavelength imaging. As a continued study, we report in this work the implementation of this anisotropic metamaterial and the experimental verification of acoustic subwavelength imaging at the zero-mass frequency.

Revisit of theoretical models. – Analyses on the transmission and reflection of a homogeneous fluid with anisotropic mass density show that either for propagating or for evanescent incident waves, the complete transmission can be achieved when the impedance matching conditions are fullfilled, which finally result in $\rho_x \to \infty$ and $\rho_z \to 0$, where ρ_x and ρ_z are, respectively, mass densities along directions parallel and vertical to the lens interface. The structure model of the lens satisfying this parameter condition has been designed, which consists of rigid slabs with a periodic array of cavities partially filled by elastic layers, as shown in fig. 1. We will show below how the lens sample can be designed and fabricated based on this theoretical model.

Sample design and fabrication. – Aluminum materials are cut into cubic blocks with the width and height equal to $a = 25\,\text{mm}$, and the thickness $h_0 = 12\,\text{mm}$. Each block is perforated with the cylindrical hole of the diameter $d_0 = 20\,\text{mm}$, serving for the guiding channel of the acoustic wave. The paper material of thickness $h_2 = 0.1\,\text{mm}$ is selected to be the elastic layer as indicated in the theoretical model. To design the unit cell of the lens, the paper membrane is sandwiched between two plastic polylactide (PLA) slabs with opening circular holes. The size of the hole determines the diameter of the vibrating membrane $d_1 = 18\,\text{mm}$. The PLA slab has the same width and height as those of the aluminum block, but a small thickness $h_1 = 1\,\text{mm}$. The sandwiched paper membrane is further attached to the perforated aluminum blocks. The combined structure builds the unit cell of the metamaterial lens, as shown in fig. 2.

The lens can be seen as an anisotropic-mass medium characterized by the dispersion relation [10]

$$\frac{k_x^2}{\rho_x} + \frac{k_y^2}{\rho_y} + \frac{k_z^2}{\rho_z} = \frac{\omega^2}{\kappa}, \tag{1}$$

where κ denotes the bulk modulus. Because of great acoustic impedance mismatching between aluminum block

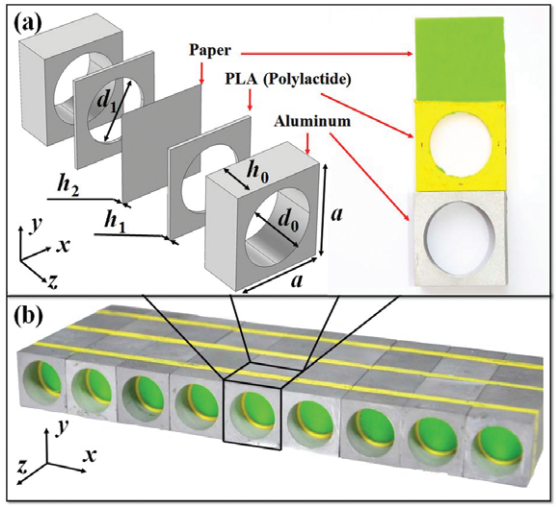

Fig. 2: (Colour on-line) (a) Schematic of the aluminum channel sandwiched paper membrane comprising the unit cell of the sample. (b) Experimental realization of the metamaterial lens with zero effective mass.

and the air, $Z_{\text{Al}}/Z_{\text{Air}} \approx 42250$, the sample is effectively rigid and motionless in the x-z plane for airborne sound, namely with infinite values of ρ_x and ρ_z. This results in the weak dependence of the propagating vector k_z on the parallel one k_x or k_y, which is the key feature of the lens for converting evanescent wave components into propagating ones [11–13].

The paper membrane has Young's modulus $E_{\text{Z}} = 2.45\,\text{GPa}$, Poission's ratio $\nu = 0.33$, and mass density $\rho = 769\,\text{kg/m}^3$ [14]. The mass density and sound velocity of the air are taken to be $\rho_0 = 1.25\,\text{kg/m}^3$ and $c_0 = 343\,\text{m/s}$. For airborne sound, the zero-mass frequency of a clamped circular plate is very close to its lowest natural frequency of the symmetric vibration, given by [15]

$$f_{\text{Lowest}} = 0.47\frac{h_2}{(d_1/2)^2}\sqrt{\frac{E_{\text{Z}}}{\rho\,(1-\nu^2)}}, \tag{2}$$

which is about 1097 Hz for the circular paper membrane used in the sample. The air wavelength corresponding to this frequency is around 313 mm, much greater than the lattice periodicity $a = 25\,\text{mm}$ and the cell thickness $h = 26.1\,\text{mm}$. Therefore, the designed sample follows the effective medium description.

The exact zero-mass frequency of the sample is determined by experimentally measuring the normal-incidence acoustic transmission with an acoustic impedance tube (Brüel&Kjær type 4206T). The transmission amplitudes measured for the samples with different number ($N = 1, 2, 3$) of unit cells are shown in fig. 3(a). The overall profile of the transmission spectrum coincides very well with the finite element simulation results shown in fig. 3(b). By using the transfer matrix method [8], we have retrieved effective mass densities of the samples and plotted them in figs. 3(c) and (d) corresponding, respectively,

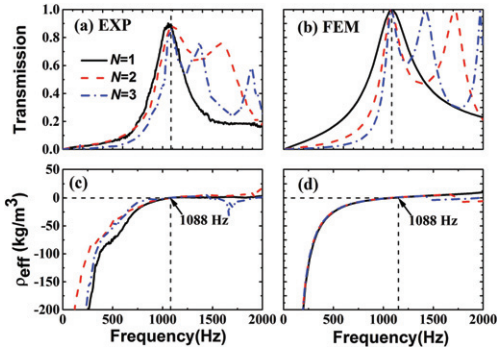

Fig. 3: (Colour on-line) (a) Experimental and (b) simulated results of normal-incidence sound transmission of the samples consisting of a different number ($N = 1, 2, 3$) of unit cells. (c), (d): their corresponding effective mass densities ρ_{eff}.

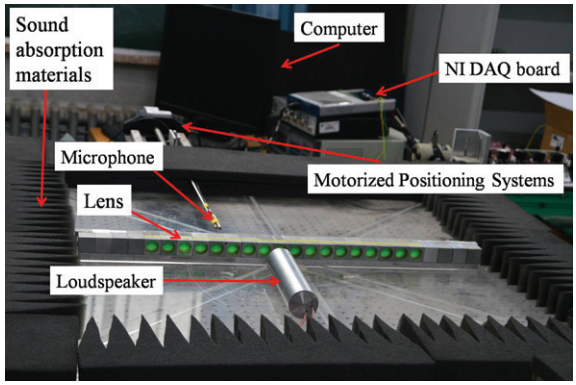

Fig. 4: (Colour on-line) Schematic diagram of the experimental setup.

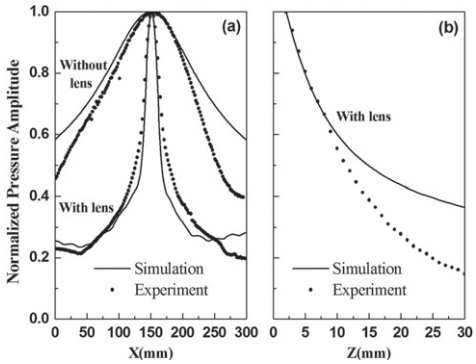

Fig. 5: (a) Experimental and simulated results of normalized pressure amplitudes along the x-direction behind the lens when one loudspeaker is placed in front of the lens. (b) Pressure amplitude distribution in the center line along the z-direction behind the lens.

to the experiment and simulation results. For all three samples, the first peak in the transmission spectrum corresponds to zero mass density at frequency 1088 Hz, which is invariant to the change of the cell numbers, namely the lens thickness. One can also find that the zero-mass frequency is quite close to the natural frequency 1097 Hz of the clamped paper membrane. This demonstrates the importance of eq. (1) to provide a preliminary prediction of the zero-mass frequency before the exact one is measured by the acoustic transmission experiment. Notice that additional transmission peaks observed in samples with $N = 2$ and 3 are due to the tunneling resonance, and the peak transmission frequencies are dependent on the number of unit cells [9]. Once the zero-mass frequency 1088 Hz is determined in the normal-incidence experiment, it is exactly the operating frequency for acoustic subwavelength imaging, since the propagating wave vector within the lens is independent of the parallel one k_x or k_y due to infinite values of ρ_x and ρ_y, as illustrated in eq. (1). It means that at this frequency, the complete transmission occurs for any oblique incident waves including evanescent ones.

Imaging experiments. – Acoustic subwavelength imaging by the fabricated sample is verified at first by the one-source experiment, in which one loudspeaker with oscillating frequency of 1088 Hz is placed in front of the lens with a distance of 2 mm. The measurement of the pressure fields behind the lens is conducted by the previously established acoustic field scanning system, as shown in fig. 4 [16]. The normalized-pressure amplitudes along the x-axis behind the lens with the distance 2 mm are measured, respectively, in the presence and absence of the lens, as shown in fig. 5(a). In contrast to the case without the lens, a sharp peak in the pressure distribution is observed when the lens is present, and the imaging resolution, defined as the full width at half-maximum (FWHM), is up to 34 mm $\approx 0.1\lambda_0$ (λ_0 is the corresponding wavelength in air), beyond the diffraction limit $0.5\lambda_0$. The finite element simulations are also conducted and found to be in good agreement with the experimental ones. Figure 5(b) shows the measured and simulated pressure amplitudes in the center line along the z-direction behind the lens. The pressure intensity attenuates rapidly as the measurement point is far away from the lens, displaying the near-field nature of the subwavelength imaging.

Further verification for acoustic subwavelength imaging is provided by placing two loudspeakers in front of the lens with the center-to-center distance of 50 mm ($\approx 0.16\lambda_0$). Figure 6 shows the measured pressure distributions behind the lens in three cases: (a) with the lens composed of one unit cell $N = 1$, (b) with and (c) without the lens composed of three unit cells $N = 3$. By comparison to the pressure distributions without the lens, two sources can be clearly resolved at the zero-mass frequency 1088 Hz by the fabricated lens consisting of either one or three unit cells.

The line distributions of the pressure amplitude behind the lens ($N = 3$) with a distance of 2 mm are plotted in figs. 7(a) and (b), corresponding, respectively, to the simulation and experiment results. It is seen that the lens can offer enough contrast to distinguish the two sources. These experiment results clearly demonstrate acoustic subwavelength imaging beyond the diffraction

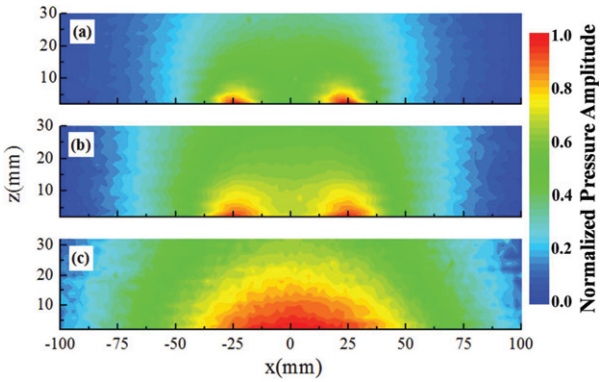

Fig. 6: (Colour on-line) Experimental results of normalized-pressure amplitude distributions behind the lens in three cases: (a) with the lens composed of one unit cell $N = 1$, (b) with and (c) without the lens composed of three unit cells $N = 3$, when two loudspeakers separated by 50 mm are placed in front of the lens.

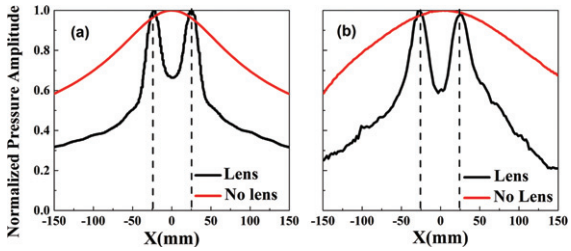

Fig. 7: (Colour on-line) (a) Simulation and (b) experiment results of the line distribution of pressure amplitudes behind the lens, when two loudspeakers separated by 50 mm are placed in front of the lens.

limit based on zero-mass metamaterials, as well as the capability of the lens for which the imaging frequency is invariant to the thickness of the lens.

As a concluding remark, we have fabricated an anisotropic zero-mass metamaterial by using the paper membrane clamped by aluminum channel structures. The natural frequency of the clamped membrane is calculated at first as an estimation of the zero-mass frequency of metamaterials, and so the geometry of the structured lens is finalized. The exact zero-mass frequency of the sample is determined by normal-incidence acoustic transmission measurement. Subwavelength imaging at this frequency is verified by both one-source and two-source experiments based on the acoustic field scanning system. The experimental results demonstrate the performance of the fabricated metamaterial samples in resolving subwavelength details below the diffraction limit. The capability of the lens for which the imaging frequency is independent of the lens thickness is also demonstrated. Applications based on such metamaterial lens can be anticipated in the areas of near-filed ultrasonic medical imaging and non-destructive evaluation.

* * *

This work was supported by the National Natural Science Foundation of China (Grant Nos. 10832002, 11172038, 11072031, and 11221202), the National Basic Research Program of China (Grant No. 2011CB610302), Program for New Century Excellent Talents in University (Grant No. NCET-11-0794) and Beijing Higher Education Young Elite Teacher Project.

REFERENCES

[1] Yao S., Zhou X. and Hu G., *New J. Phys.*, **10** (2008) 043020.
[2] Craster Richard V. and Guenneau Sebastien (Editors), *Acoustic Metamaterials* (Springer) 2012.
[3] Deymier Pierre (Editors), *Acoustic Metamaterials and Phononic Crystals* (Springer) 2013.
[4] Zhou X. and Hu G., *Appl. Phys. Lett.*, **98** (2011) 263510.
[5] Fleury R. and Alù A., *Phys. Rev. Lett.*, **111** (2013) 055501.
[6] Park J. J., Lee K. J. B., Wright O. B., Jung M. K. and Lee S. H., *Phys. Rev. Lett.*, **110** (2013) 244302.
[7] Yao S., Zhou X. and Hu G., *New J. Phys.*, **12** (2010) 103025.
[8] Li P., Yao S., Zhou X., Huang G. and Hu G., *J. Acoust. Soc. Am.*, **135** (2014) 1844.
[9] Liu A., Zhou X., Huang G. and Hu G., *J. Acoust. Soc. Am.*, **132** (2012) 2800.
[10] Torrent D. and Sánchez-Dehesa J., *Phys. Rev. Lett.*, **105** (2010) 174301.
[11] Jia H., Ke M., Hao R., Ye Y., Liu F. and Liu Z., *Appl. Phys. Lett.*, **97** (2010) 173507.
[12] Liu F., Cai F., Peng S., Hao R., Ke M. and Liu Z., *Phys. Rev. E*, **80** (2009) 026603.
[13] Zhu J., Christensen J., Jung J., Martin Moreno L., Yin X., Fok L., Zhang X. and Garcia-Vidal F. J., *Nat. Phys.*, **7** (2011) 52.
[14] C. E. S. Selector 4.0, `http://www.grantadesign.com/products/ces/`.
[15] Kinsler L. E., Frey A. R., Coppens A. B. and Sanders J. V., *Fundamentals of Acoustics*, 4th edition (Wiley, New York) 1999.
[16] Su H., Zhou X., Xu X. and Hu G., *J. Acoust. Soc. Am.*, **135** (2014) 1686.